Comparing horizontal path C_n^2 measurements over 0.6 km in the tropical littoral environment and in the desert

Mark P. J. L. Chang[1], Carlos O. Font[2], G. Charmaine Gilbreath[2], Eun Oh[2],
Emi Distefano[2], Sergio Restaino[3], Christopher Wilcox[3] and Freddie Santiago[4]

[1]Physics Department, University of Puerto Rico, Mayagüez, Puerto Rico 00680.
[2]U.S. Naval Research Laboratory, Washington D.C. 20375.
[3]U.S. Naval Research Laboratory West, Albuquerque, New Mexico.
[4]P.O. Box 2114, Guaynabo, PR 00970-2114.

ABSTRACT

We have measured the optical turbulence structure parameter, C_n^2, in two extremely different locations: the first being the littoral region on the southwest coast of Puerto Rico. The second location is over the dry desert in central New Mexico. In both cases, the horizontal beam paths are approximately 0.6 km long, within 2 meters of the local surface (Puerto Rico) and varying between 2 to 100 meters (New Mexico). We present our findings from the two datasets.

Keywords: Strength of Turbulence Parameter, Scintillation, Littoral Turbulence, Desert Turbulence

1. INTRODUCTION

We have obtained weak turbulence optical C_n^2 measurements, integrated over 600m horizontal paths in both the littoral environment in the Caribbean region (southwest Puerto Rico) and in the high desert of central New Mexico. The Puerto Rico littoral data record covers the period between February 4 to March 13, 2007 (year days 35 to 72). The New Mexico record is more limited, covering only March 5 to March 9, 2007 (year days 95 to 99). The instrument systems used are identical OSI LOA-004s, described in previous reports.[1–3]

For convenience, we designate the littoral measurement campaign as VIPh in this paper; results of a previous (2006) campaign at the same site have been reported recently.[4] The New Mexico measurements took place at the Starfire Optical Range, Albuquerque and we reference them with the abbreviation SOR.

The robust and repeatable mathematical properties of a variable are sometimes referred to as "stylised facts". In this paper we seek to establish some of the stylised facts of our observations; the structure of the document is as follows: In Section 2 we present a summary of the VIPh measurements over the 37 days and what we have learned from this record. We follow this with a discussion of the 5 days of desert measurements. We observe the expected temperature driven characteristics of weak, clear air turbulence in the time series measurements. In particular, we note that the SOR system exhibits features of a lognormal amplitude distribution throughout the entire record whereas the VIPh system is modified by a daytime component. In general we are concerned with understanding these systems from the perspective of scaling. By identifying characteristic scales or scale–independent features, we will be better placed to discuss the various underlying physical processes contributing to the system variations. Moreover, quantitative comparitive studies between the time series records can be made. With that in mind, we have analysed first and second order statistics. Specifically, we examine the first difference (or single decimation) of the C_n^2 measurements, the probability distribution function (PDF), the autocorrelation function (ACF) and the Hilbert Huang spectra. We list the observed stylised facts in Section 3 and then conclude with Section 4.

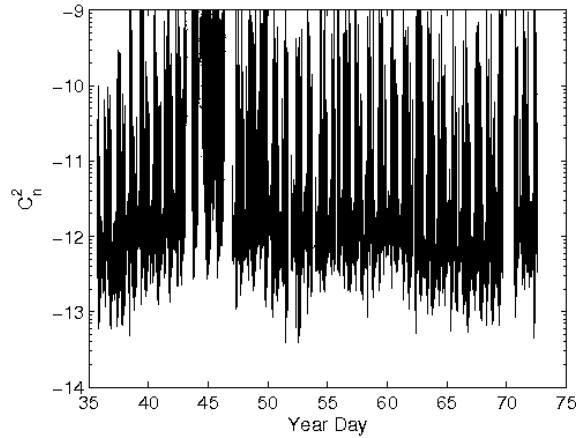Further author information: (Send correspondence to M.P.J.L.C.)
M.P.J.L.C.: E-mail: mark@charma.uprm.edu, Telephone: 1 787 265 3844

		Form Approved OMB No. 0704-0188

Report Documentation Page

1. REPORT DATE **2007**	2. REPORT TYPE	3. DATES COVERED **00-00-2007 to 00-00-2007**

4. TITLE AND SUBTITLE	5a. CONTRACT NUMBER
Comparing horizontal path C2n measurements over 0.6 km in the tropical littoral environment and in the desert	5b. GRANT NUMBER
	5c. PROGRAM ELEMENT NUMBER
6. AUTHOR(S)	5d. PROJECT NUMBER
	5e. TASK NUMBER
	5f. WORK UNIT NUMBER

7. PERFORMING ORGANIZATION NAME(S) AND ADDRESS(ES) **Naval Research Laboratory,Code 8123, Advanced Systems Technology Branch,4555 Overlook Ave SW,Washington,DC,20375**	8. PERFORMING ORGANIZATION REPORT NUMBER

9. SPONSORING/MONITORING AGENCY NAME(S) AND ADDRESS(ES)	10. SPONSOR/MONITOR'S ACRONYM(S)
	11. SPONSOR/MONITOR'S REPORT NUMBER(S)

12. DISTRIBUTION/AVAILABILITY STATEMENT
Approved for public release; distribution unlimited

13. SUPPLEMENTARY NOTES

14. ABSTRACT
We have measured the optical turbulence structure parameter, C2n , in two extremely different locations: the first being the littoral region on the southwest coast of Puerto Rico. The second location is over the dry desert in central New Mexico. In both cases, the horizontal beam paths are approximately 0.6 km long, within 2 meters of the local surface (Puerto Rico) and varying between 2 to 100 meters (New Mexico). We present our findings from the two datasets.

15. SUBJECT TERMS

16. SECURITY CLASSIFICATION OF:			17. LIMITATION OF ABSTRACT	18. NUMBER OF PAGES	19a. NAME OF RESPONSIBLE PERSON
a. REPORT **unclassified**	b. ABSTRACT **unclassified**	c. THIS PAGE **unclassified**	**Same as Report (SAR)**	**9**	

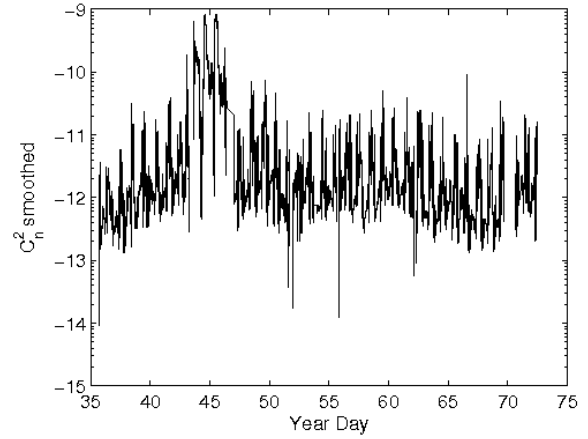**Standard Form 298 (Rev. 8-98)**
Prescribed by ANSI Std Z39-18

2. DATA

2.1. VIPh (Puerto Rico) record

The near–infrared probe beam for these measurements was positioned at a mean height of 1.5 m above sea level, aligned along a nearly North–South path of approximately 600 m length. The transmitter and receiver systems were placed at fixed locations on jettys for 32 out of the 37 campaign days (for more details on the dockside geometry, see Chang et al (2007)[4]). During the other 5 days, year days 43 to 47, the receiver system was placed on a moored, floating platform within 10 m to the south of its fixed position, with the aim of testing the stability of its tripod mount in the presence of light tidal and wash effects. Although these 5 days' worth of readings have a large C_n^2 baseline offset relative to the remaining days, we nevertheless include them in the discussion as they provide visual continuity in Figs. 1 and 2.

Figure 1. The complete record of measurements over 37 days for the VIPh campaign. Here, as in all subsequent graphs, the integer day indicates midnight local time.

Figure 2. The same data as Fig. 1, smoothed with a forward rolling average of 120 points including the data gaps. Year days 42 to 47 clearly show the effect of placing the scintillometer receiver on a floating platform. There is a strong, slow modulation on the baseline. The physical cause of this modulation will be explored elsewhere.
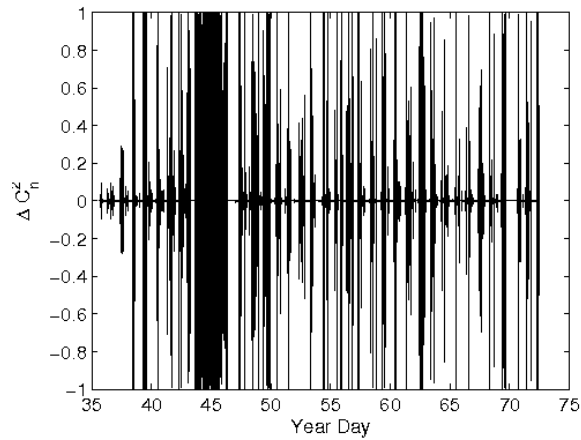
2.1.1. First Order Statistics: Differencing and PDF

The first difference of the C_n^2 measures, Fig. 3 shows "bursts" in the signal, where each burst correlates with the daylight hours per day. Year days 43 to 47 also stand out as having large pointwise differences; this is due to the mechanical instability of the floating platform compared to the fixed jetty locations on the other days. There is possibly a slowly varying envelope across the daytime bursts, although this is highly unclear due to the variation in the larger amplitudes of the time series. To minimise the effect of this variation, we determined the first difference of the $\log C_n^2$ values, Fig. 4. From Fig. 4 we note the daytime modulation on the envelope of the $\log C_n^2$ difference. This modifies the underlying nighttime lognormal C_n^2 probability distribution function (PDF). Fig. 5 shows that the C_n^2 PDF would be well fit with a bi–modal distribution.
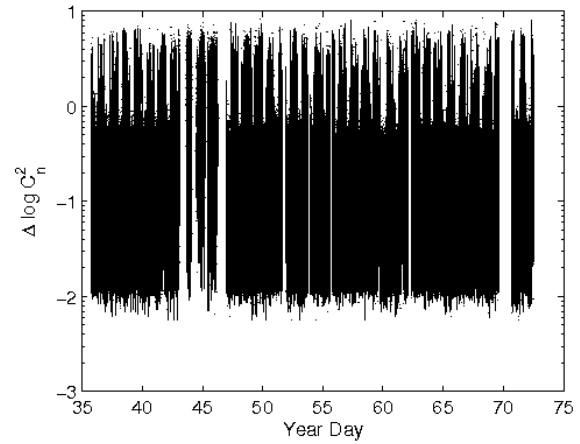
2.1.2. Second Order Statistics: ACF and Hilbert Huang Spectrograph

The range of amplitudes present in the C_n^2 record is described by the PDF; the range of temporal periods can be found by examining the autocorrelation function (ACF). This is defined as
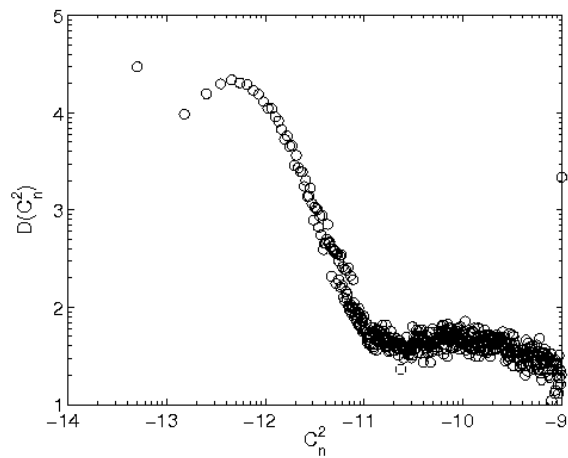
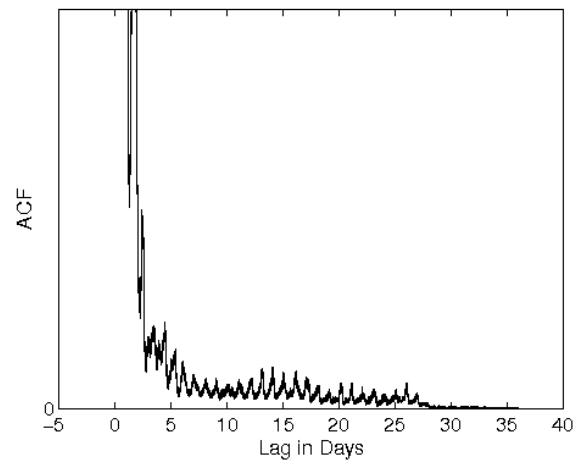$$ACF(\tau) = \sum_t C_n^2(t) C_n^2(t + \tau) \tag{1}$$

Figure 3. ΔC_n^2 (single sample decimation) for the VIPh data; note a possible modulation on the amplitude envelope.

Figure 4. $\Delta \log C_n^2$ (single sample decimation) for the VIPh data; a rapidly modulated upper envelope can be clearly discerned, showing the daytime effects upon the data.

Figure 5. PDF of the VIPh C_n^2 data record, using 10 000 bins, showing that a bi–modal fit is very appropriate.
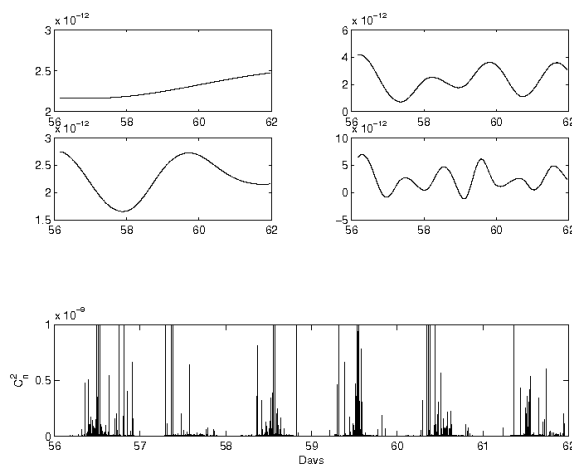

Figure 6. ACF of the VIPh C_n^2 data record, truncated on the vertical axis.

We show this in Fig. 6. The modulation atop the basic trend is again due to the solar heating during the daylight hours. The ACF initially shows a rapidly dropping exponential followed by a long–range tail.

The frequency space version of the ACF is much less trivial to produce. The main obstacle is the non–stationarity of the time series, which does not allow us to use conventional algorithms such as the Fourier Transform directly on the data.[2] By windowing the data into "stationary" subsets as in Short Time Fourier Transform techniques, it is possible to calculate a frequency map with a Fourier basis. However this tends to have aliasing and resolution problems, since the basis representation is predefined. Fortunately the Hilbert Huang Transform[5] improves on this by defining the basis adaptively from the given time series via Empirical Mode Decomposition. The components of the adaptive basis are known as the Intrinsic Mode Functions (IMFs).

The full data set has a large number of data gaps, primarily due to mechanical misalignments as the instrumentation was unattended for long periods. Rather like the aliasing problem in Fourier methods, Empirical Mode Decomposition is very sensitive to long breaks in the data stream,[6] so the raw data is not ideal for spectral processing. We have therefore limited our spectral study to a subsection with few gaps.
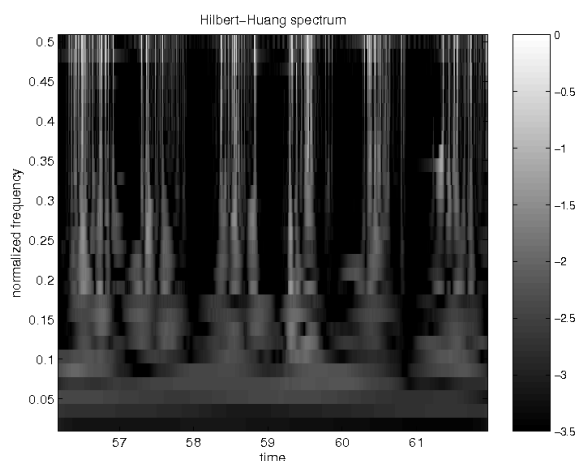
We show a 5×10^5 point subset of the data (covering approximately 6 days) in Fig. 7, in which the level of lost data is less than 5%. 30 components were determined from the data (29 IMFs and trend), which are notable by their division into 3 main orders of magnitude amplitude–wise: 10^{-10} (10 highest frequency IMFs), 10^{-11} (next 15 IMFs) and 10^{-12} m$^{-2/3}$ (lowest frequency IMFs and trend). The IMFs allow us to find a map
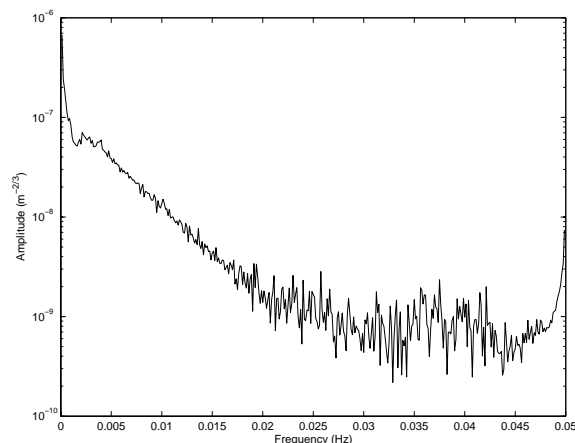

Figure 7. VIPh C_n^2 data subset: [Upper panel] (Top to bottom, left to right) The trend; trend + lowest frequency IMF; trend + 2 lowest frequency IMFs; trend + 3 lowest frequency IMFs. [Lower panel] The data subset used for spectral analysis.

of instantaneous frequencies; this in turn generates the Hilbert Huang spectrogram (HHS). The HHS is a high resolution map in the time–frequency–amplitude domain, similar to a wavelet spectrogram. Fig. 8 shows the HHS for the data subset. We see that below approximately 5×10^{-3} Hz, the amplitudes are spread evenly across all time bins. Above this, the C_n^2 amplitudes are bunched into what is clearly the effect of solar insolation upon the distribution.

The HHS map can be simplified by summing over the time axis to produce the (temporal) marginal Hilbert Huang spectrum (Fig. 9). Though suggestive of a Fourier power spectrum, the points on the marginal spectrum represent the local probability of occurance of the frequencies. The curve has three major regions: (1) a decreasing ramp down to about 0.025 Hz, (2) a floor between 0.025 to 0.045 Hz and (3) a steep rise. Region (1) is potentially representative of the atmospheric activity in the absence of the Sun, being similar to Fig. 18. Region (2) is likely to be the result of the Sun's action on the airmass. Region (3) is probably the result of numerical and/or instrumental noise, including the effect of the data gaps.
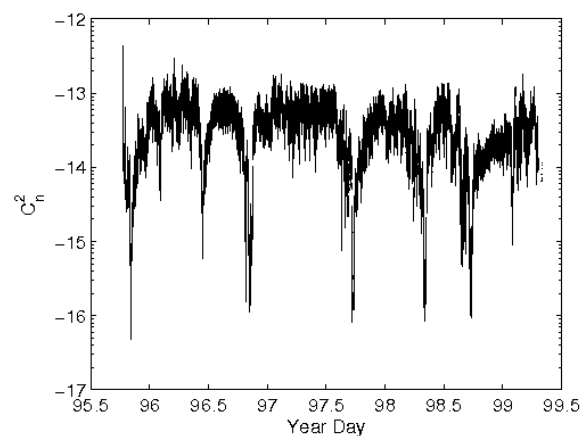
Figure 8. Hilbert Huang Spectrogram of the VIPh C_n^2 data record. The frequencies are normalised with respect to the sample rate (0.1 Hz) and the vertical greyscale key denotes the exponent$\times 10^{-1}$ of the logarithmic amplitude scale.
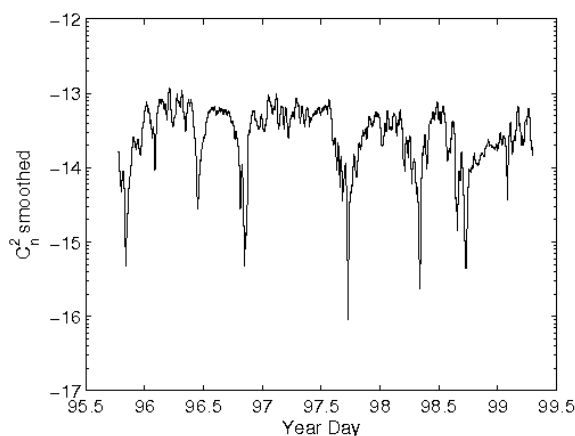

Figure 9. The Marginal Spectrum found by summing Fig. 8 over time. Note the 3 major components to the curve.

2.2. SOR (New Mexico) record

The probe beam was positioned at a mean height of 1 m above ground level at the receiver and transmitter ends, again aligned along a nearly North–South path of approximately 600 m length. The uneven intervening terrain caused beam altitude variations of up to 100 m along the path. Logistical considerations prevented a longer set from being obtained, although we fully intend to extend these data in the future. At first glance Figs. 10 and

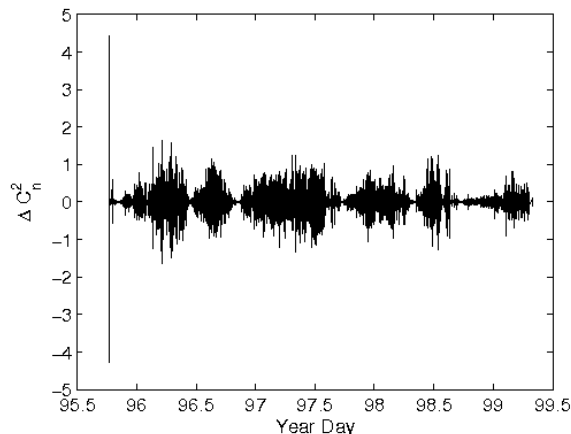**Figure 10.** The complete record of SOR measurements over 5 days.

Figure 11. The SOR data smoothed with a forward rolling average of 120 points, which also includes the data gaps.
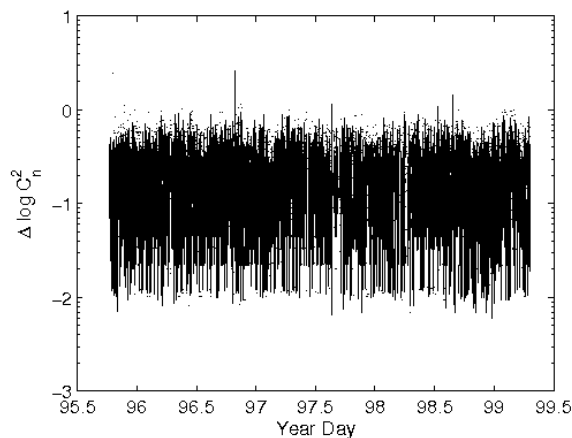
11 show a lack of pronounced daytime "bump" in the logarithmic SOR time series; this is a manifestation of the well known temperature dependence of C_n^2 as temperatures were much lower than the VIPh environment. This is also evidenced in the lower mean value of C_n^2. We observe that the minima are much more pronounced here than for the VIPh record, though we cannot determine if this is a temporally local effect or it is more global in scope.

2.2.1. First Order Statistics: Differencing and PDF

As with the VIPh record, the first difference of the C_n^2 measures shows burst activity in the signal, Fig. 12 (a). This "burstiness" can result from critical phenomenae, or simply from data with a fractional lognormal amplitude distribution (which is equivalent to fractional Brownian motion). To distinguish between these possibilities, we again calculated the first difference in $\log C_n^2$ values. It is instructive to examine the PDF,
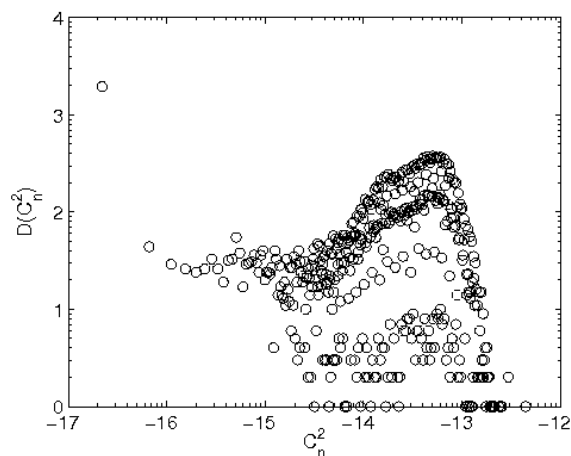

Figure 12. ΔC_n^2 (single sample decimation) for SOR, showing a strong modulation on the amplitude envelope ("burstiness").
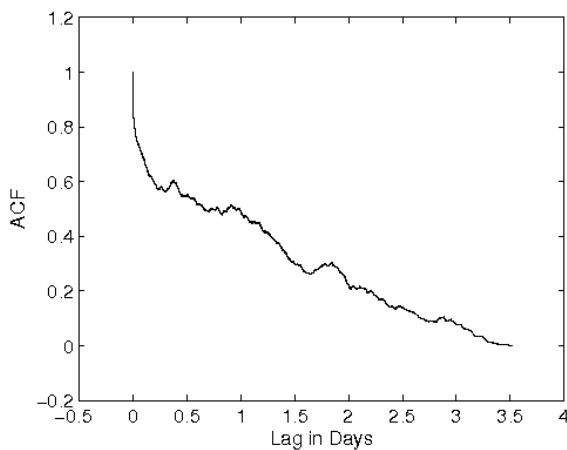

Figure 13. $\Delta \log_e C_n^2$ (single sample decimation) for SOR, which shows a more or less constant behaviour. Thus the amplitude modulation from Fig. 12 is an effect of a fractional lognormal distribution.

shown in Fig. 14. While a single lognormal curve would seemingly fit the PDF, it is apparent that there are modifying effects giving it a skewed, platykurtic shape.

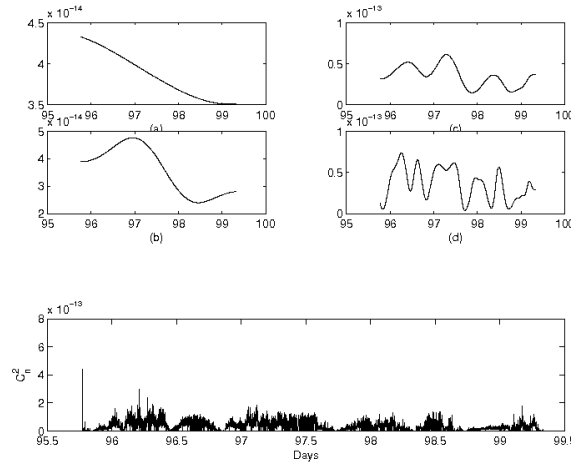**Figure 14.** PDF of the SOR C_n^2 data record, using 10 000 bins.

Figure 15. ACF of the SOR C_n^2 data record, showing qualitatively that there is an exponential decrease, followed by a long range tail.

2.2.2. Second Order Statistics: ACF

Fig. 15 shows the normalised ACF for the SOR record. The modulation atop the basic trend may be due to the minimal solar heating of the air during the daylight hours, which would generally leave the air warmer than the ground. The trend of this ACF is a single component curve, being only a long range tail.

The frequency domain version was again found through the use of the Hilbert Huang Transform algorithm. Approximately 5% of the record is comprised of data gaps. Since their effect upon the spectrogram is negligible (see Appendix A), we show the results of analysing the raw data. The IMFs indicate two ranges of oscillation

Figure 16. [Upper Panel] (Top to bottom, left to right) Trend, trend + lowest frequency IMF, trend + 2 lowest frequency IMFs and trend + 3 lowest frequency IMFs. [Lower panel] SOR C_n^2 raw data.

amplitude, 10^{-13} and 10^{-14} m$^{-2/3}$. The diurnal solar cycle's effect can be seen in the low frequency IMFs.
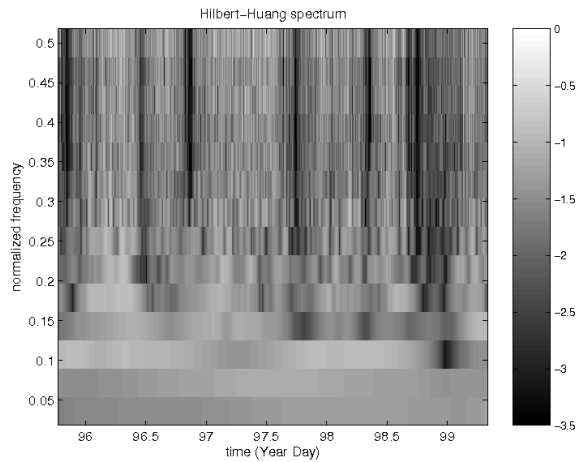
From the IMFs we obtain the Hilbert Huang spectrogram, shown in Fig. 17, and the marginal spectrum (Fig. 18). The spectrogram gives a clear indication that most of the amplitudes in the data lies in the lower frequencies, as expected. The location of the minima in the lower frequency ranges are clearly marked. Although no frequency modulation can be seen, a division between frequency bands can be seen in the spectrogram, delineated by those frequencies which have strong amplitude minima and those which do not. We emphasise that the marginal spectrum is the integrated projection onto the frequency axis of the spectrogram's data. This shows a long exponential tail; the meaning of the marginal spectrum is that the amplitude of each frequency represents a probability of appearance somewhere in the time series. The slight rise at the highest frequencies may be due to sampling error and is certainly influenced by the data holes.

3. STYLISED FACTS
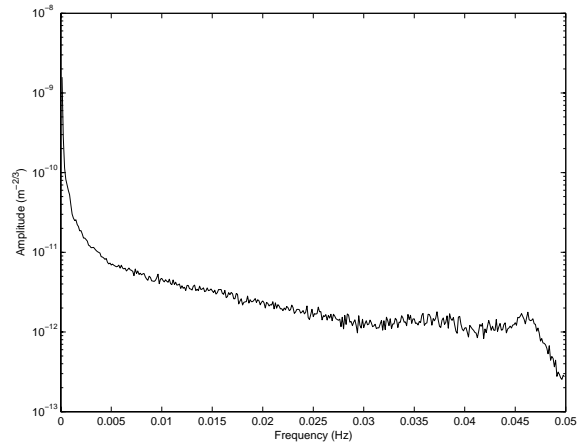
The stylised facts that can be compiled from our observations are as follows:

3.0.3. VIPh

- The complete record shows a clear daytime heating and cooling effect, on top of the nighttime turbulence record.

- The baseline of the VIPh time series has a modulation.

- These two effects show themselves as a bimodal distribution, where one component is possibly lognormal and the other is strongly gaussian.

- The ACF is a strong exponential decay, with riding waves on top representing the diurnal heating of solar insolation.

- The contiguous subsection's marginal spectrum shows two components corresponding to background/nighttime and daytime.

Figure 17. Hilbert Huang Spectrogram of the SOR C_n^2 data record. The frequencies are normalised with respect to the sample rate (0.1 Hz) and the vertical greyscale key shows the exponent×10^{-1} of the logarithmic amplitude scale.

Figure 18. Marginal Spectrum found by summing Fig. 17 over time.

3.0.4. SOR

- The 5 day record shows little or no daytime heating effect, and the minima are much deeper than for VIPh measurements.

- The PDF is approximately represented by a single lognormal, although there is finite skew and kurtosis.

- The marginal spectrum shows a long, slow decay with very few features.

The next stage of analysis will be to determine which aspects of the data, if any, are scale dependent or scale–free. Through this, we should be able to identify direct or even indirect physical drivers of the changes in the strength of turbulence parameter that we are measuring.
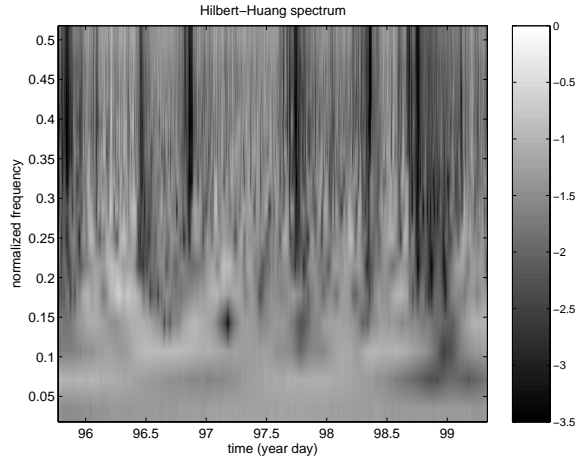
4. CONCLUSIONS

We have presented weak turbulence data collected using identical commercial scintillometers over 600 m horizontal paths in two different environments. From an initial analysis, we have found a number of features that have been summarized as "stylised facts". We have demonstrated that the theoretical lognormal distribution is modified somewhat in both a cold, dry region and a warm, humid locale. As could be expected, the SOR data has a lower mean than the VIPh record since the winter desert is some 30 to 50° F colder than the tropical shore. One unexplained occurance is the much deeper C_n^2 parameter minimum seen in the desert data than in the tropical, littoral record, which is not accounted for in any theory.
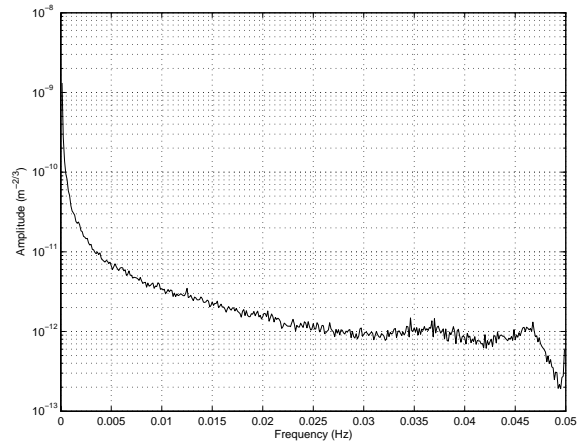
ACKNOWLEDGMENTS

APPENDIX A.

As proof that the 5% level of data holes has minimal effect on the Hilbert Huang analysis, we show the spectrogram and marginal spectrum of the SOR data filled using an ARIMA(0,$d = 0.5$,0) algorithm. A small growth in the highest frequencies are noticeable, due principally to the lack of edge continuity but there are few other differences.

Figure 19. Hilbert Huang Spectrogram of the SOR C_n^2 data record. Compare to Fig. 17.

Figure 20. Marginal Spectrum found by summing Fig. 19 over time. Compare to Fig. 18.

REFERENCES

1. M. P. J. L. Chang, E. A. Roura, C. O. Font, G. C. Gilbreath, and E. Oh, "Applying the hilbert-huang decomposition to horizontal light propagation c_n^2," in *Advances in Stellar Interferometry*, J. D. Monnier, M. Schller, and W. C. Danchi, eds., *Proc. SPIE* **6268**, 2006.
2. M. P. J. L. Chang, C. O. Font, G. C. Gilbreath, and E. Oh, "Humidity's influence on visible region refractive index structure parameter C_n^2," *Applied Optics (in press), ArXiv Physics e-prints* **physics/0606075**, June 2006.
3. C. O. Font, "Understanding the atmospheric turbulence structure parameter C_n^2 in the littoral regime," Master's thesis, University of Puerto Rico at Mayagüez, 2006.
4. M. P. J. L. Chang, C. O. Font, G. C. Gilbreath, and E. Oh, "Humidity contribution to cn2 over a 600m pathlength in a tropical marine environment," in *Free–Space Laser Communication Technologies XIX and Atmospheric Propagation of Electromagnetic Waves*, S. Mecherle and O. Korotkova, eds., *Proc. SPIE* **6457**, 2007.
5. N. E. Huang, Z. Shen, S. R. Long, M. C. Wu, H. H. Shih, Q. Zheng, N.-C. Yen, C. C. Tung, and H. H. Liu, "The empirical mode decomposition and the Hilbert spectrum for nonlinear and non-stationary time series analysis," *Proc. R. Soc. Lond. Ser. A* **454**, pp. 903–995, 1998.
6. M. P. J. L. Chang, H. Nazari, C. O. Font, G. C. Gilbreath, and E. Oh, "Patching c_n^2 time series data hole using principal component analysis," in *Atmospheric Propagation IV*, C. Young and G. C. Gilbreath, eds., *Proc. SPIE* **6551**, 2007.